80-GT-111

AN ASME PUBLICATION
$50.00 per copy $1.00 to ASME Members

THE AMERICAN SOCIETY OF MECHANICAL ENGINEERS
345 E 47 St., New York, N.Y. 10017

Turbulence Amplification in Flow about an Airfoil

W. Z. Sadeh
Professor,
Engineering and Fluid Mechanics,
Dept. of Civil Engineering,
Mem. ASME

P. P. Sullivan
Research Assistant

Colorado State University,
Fort Collins, Colo.

An experimental investigation of the evolution of freestream turbulence in flow about an airfoil was conducted in order to ascertain its selective amplification induced by the stretching mechanism according to the vorticity-amplification theory. Significant amplification of the streamwise turbulent energy transpired even in the limiting flow situation studied of a symmetric airfoil at zero angle of attack where the stretching is the least. Substantiation of the stretching effect was provided by the almost 100 percent amplification of turbulence with respect to its background level in the absence of the airfoil. Realization of preferred amplification at scales larger than the neutral scale of the stagnation flow was clearly indicated by the variation of the discrete streamwise turbulent energy. Particularly important was the detection of a most amplified scale which is characteristic of the coherent substructure near the airfoil stagnation zone and, concurrently, commensurate with the boundary-layer thickness.

NOMENCLATURE

A_e	amplification factor
a	stagnation flow constant
B	hot-wire parameter
c	airfoil chord
d	rod diameter
E	DC output voltage
E_o	DC output voltage in still air
e	fluctuating voltage
M	mesh length
m	flow factor
Re_c	profile-chord Reynolds number
Re_d	rod-diameter Reynolds number
Re_M	grid-mesh Reynolds number
Tu	turbulence intensity
U	total (Sect. 2) or mean velocity
u	turbulent velocity
u^2	mean-square value of turbulent velocity
$u_2^2(\lambda)$	discrete streamwise turbulent energy
x_i	Cartesian coordinates
x_{2g}	grid position
x_2'	longitudinal distance measured from grid
δ	boundary-layer thickness
ε	airfoil thickness parameter
η	dimensionless length
λ	scale
λ_o	neutral scale
λ_m	most amplified scale
ν	kinematic viscosity
ω	vorticity

Subscripts

1,2,3	Cartesian coordinates
∞	freestream
o	reference station
b	background
L	laminar
min	minimum
rms	root-mean-square

Superscripts

$\vec{}$	means "vector"
^{o}, $'$, $''$, $'''$	means "streamwise station"
$\bar{}$	time-averaged value
$\sim$	dimensionless quantity

1. INTRODUCTION

The importance of the amplification of freestream turbulence at particular scales in flow about a bluff body is at the present time widely acknowledged. Results of many experimental and theoretical studies testify to the strong sensitivity of stagnation-point skin friction and heat transfer to the presence of turbulence and, particularly, to the scale distribution of the turbulent energy. The occurrence of relatively large velocity fluctuations near the front stagnation zone of a circular cylinder was first reported in 1928 by Piercy and Richardson [1]. An early review of this flow can be found in a report by Kestin and Maeder [2]. More recent theoretical analyses and experimental studies of turbulence amplification are presented in papers by Sutera, Maeder and Kestin [3], Sutera [4], Sadeh, Sutera and Maeder [5,6], Kestin and Wood [7], Bearman [8], Hunt [9], Traci and Wilcox [10], Sadeh and Brauer [11], to mention a few. It was further found that the laminar boundary layer and its separation angle on a circular cylinder are significantly influenced by amplified turbulence

Contributed by the Gas Turbine Division of The American Society of Mechanical Engineers for presentation at the Gas Turbine Conference & Products Show, New Orleans, La., March 10-13, 1980. Manuscript received at ASME Headquarters December 26, 1979.

Copies will be available until December 1, 1980.

concentrated at scales commensurate with the thickness of the prevalent boundary layer [12]. Interaction of the amplified turbulence with the boundary layer induced its change from laminar to turbulent. This drastic modification of the boundary layer at subcritical Reynolds numbers led, in a manageable way, to separation angles and drag coefficients attainable only at much higher supercritical Reynolds numbers.

Amplification of freestream turbulence in flow around a streamline body, such as an airfoil, or in flow through a blade cascade has not yet been explored. Occurrence of relatively high turbulence near the front stagnation point of an airfoil at a profile-chord Reynolds number of 4×10^4 was first observed by Piercy and Richardson in 1930 [13] but since then investigation of this important flow situation has remained dormant. Selective amplification of turbulence in flow about an airfoil, similar to that observed in flow around a circular cylinder, is likely to transpire under appropriate freestream turbulent energy conditions. The amplified turbulence possesses further the potential to inhibit and even to fully forestall laminar separation on the profile suction side provided that it is concentrated at scales capable of interacting with the boundary layer. This practical consequence of the amplification of turbulence at selected scales has not yet been studied.

Exploratory experimental investigations of the effect of turbulence intensity in flow through a stationary blade cascade at subcritical blade-chord Reynolds numbers of 9×10^4 and 1.6×10^5 were recently conducted by Schlichting and Das [14] and Kiock [15]. Restriction and even forestalling of laminar separation on the blade suction side along with reduction in the cascade aerodynamic losses were obtained within a narrow range of low intensity of superimposed turbulence in the oncoming stream. With increasing level of superimposed turbulence intensity beyond a certain critical value of about 3%, the initial aerodynamic losses were, however, restored. This behavior can be, in all likelihood, attributed to the particular scale distribution of turbulent energy in these experiments but no information about it is reported in these two papers.

The primary goal of the present investigation was to examine the amplification of freestream turbulence in flow about a single airfoil at subcritical Reynolds numbers ranging from 5×10^4 to 2×10^5. To this end, it was sensible to first investigate the amplification of oncoming turbulence in flow around a single symmetric airfoil in order to avoid profile form effects. This effort represents the first phase of a long-term investigation devoted to determining the selective amplification of turbulence and the effect of the amplified turbulence in flow through a blade cascade.

The amplification of turbulence in flow about a body is governed by the stretching of cross-vortex tubes as they approach the body stagnation zone according to the vorticity-amplification theory [3,5]. This theory is therefore briefly reviewed below in order to explicate the guidelines that directed this investigation.

2. VORTICITY-AMPLIFICATION THEORY

A satisfactory explanation for the amplification of freestream turbulence in flow around a body and the subsequent effect of the amplified turbulence upon the body boundary layer is offered by the vorticity-amplification theory advanced by Sutera et al. [3] and Sadeh et al. [5]. This theory suggests that cross vorticity present in a stream, no matter how small initially, is susceptible to undergoing significant amplification at particular scales as it is conveyed by the diverging mean flow toward a body stagnation zone. Stretching of cross-vortex tubes is proposed as the mechanism responsible for the amplification of cross vorticity and, hence, of streamwise turbulence. Amplification occurs selectively at scales λ larger than a certain neutral scale λ_o. At scales smaller than the neutral one, on the contrary, the cross vorticity dissipates more rapidly than it amplifies owing to the viscous action.

Crossflow about a symmetric two-dimensional airfoil of chord c disregarding viscous dissipation is examined in order to describe the stretching mechanism. It is further assumed that the approaching total velocity U_2 contains mainly cross vorticity ω_1 susceptible to undergoing amplification by stretching. This flow situation for a single ideal cross-vortex tube of a scale λ larger than the neutral one initially oriented in the x_1-direction at some upwind distance x_2^o from the airfoil leading edge along with the system of coordinates used is portrayed in Fig. 1. As this cross-vortex tube is conveyed by the mean flow toward the airfoil stagnation zone, it experiences simultaneous pure axial stretching and streamwise biased tilting as shown in Fig. 1. The pure axial stretching is governed by the positive rate of tensile strain $\partial U_1/\partial x_1$. On the other hand, the

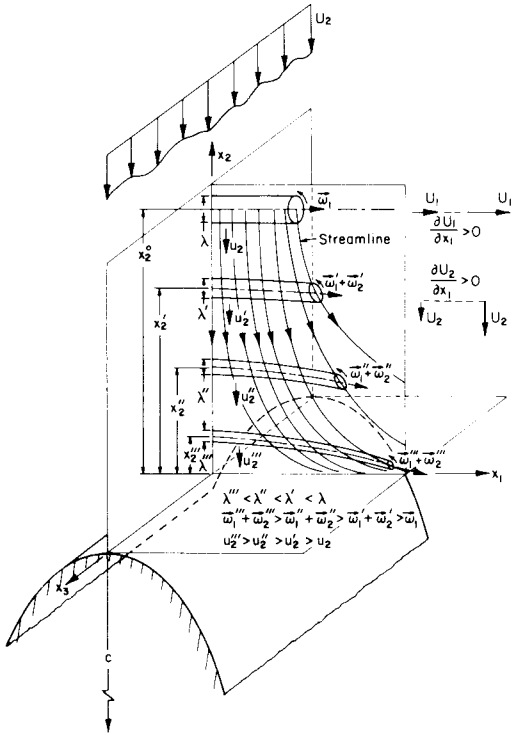

Fig. 1 Stretching and tilting of a cross-vortex tube in flow about an airfoil.

streamwise biased tilting is controlled by the favorable rate of cross strain $\partial U_2/\partial x_1$ whose magnitude increases in the x_1-direction. These two

suitable rates of strain are, in turn, effected by the diverging mean flow. Each cross-vortex tube undergoes additional significant axial stretching and acquires an axial vorticity component ω_2 in the x_2-direction as a consequence of its streamwise biased tilting. Both the volume and angular momentum of each cross-vortex tube are conserved throughout its stretching and tilting as a result of neglecting the viscous dissipation. Stretching (or elongation) of a cross-vortex tube leads consequently to a decrease in its scale λ and an increase in its vorticity $\vec{\omega}_1 + \vec{\omega}_2$. Then the streamwise turbulent velocity u_2 in the plane normal to the cross-vortex tube axis amplifies and turbulent kinetic energy accumulates within the stretched cross-vortex filament. The decrease in the scale and the concurrent increase in the vorticity of a cross-vortex tube nearing the stagnation zone of an airfoil along with the accompanying amplification of the streamwise turbulent velocity are illustrated in Fig. 1 at several streamwise stations x_2^s, x_2^t, x_2'' and x_2'''.

The stretching and tilting lead to the emergence of an organized cellular flow pattern near the stagnation zone of a body [3,5,11]. This coherent substructure consists ideally of a regular array of standing cross-vortex tubes of equal scale distributed spanwise and with their cores outside the body boundary layer. Within the cells of this regular array of energy-containing eddies, the rotation alternates in its direction and turbulent energy accumulates. Most of the turbulence amplification occurs at a most amplified scale λ_m [6] characteristic of the coherent substructure. This most amplified scale is generally greater than but commensurate with the thickness of the body boundary layer. Discrete vortices (or eddies) are continuously drawn out from this array of energy-containing eddies and, subsequently, swept downstream by the main flow around the body. Penetration of these energized vortices into the prevalent boundary layer leads to arresting the growth or even to forestalling the onset of laminar separation by promoting the development of a turbulent boundary layer. One can thus affect the nature of a body boundary layer at subcritical Reynolds numbers in a controlled way provided that the amplification of freestream turbulence is adequately managed by means of the stretching and tilting mechanisms.

It is of utmost importance to stress that the stretching of cross-vortex tubes in flow about an airfoil at zero and/or a small angle of attack is dominated by their streamwise biased tilting. Pure axial stretching is less significant in flow about an airfoil than in flow about a bluff body. This is due to the curvature of its nose and the resulting fast rate of flow divergence around it. The stretching in flow about an airfoil occurs then at much smaller spatial scales and much more rapidly than in flow about a circular cylinder.

3. EXPERIMENTAL SETUP

The experimental investigation reported herein was conducted in a 1.83x1.83x27 m (6x6x88 ft) low-speed closed-circuit single-return wind tunnel at the Fluid Dynamics and Diffusion Laboratory, Colorado State University. Stable airspeeds from less than 0.3 up to about 36 m/s (1 to 120 ft/s) are generated in this wind tunnel by a 4-blade propeller driven by a 400 hp DC motor. The airspeed can be varied continuously with a resolution better than about 5% by adjusting the pitch of the propeller blades and/or the motor speed. In this wind tunnel the background freestream turbulence intensity, based on the local mean velocity, is never larger than about 0.7% at all airspeeds.

A two-dimensional symmetric NACA 65-010 airfoil of 122 cm (4 ft) chord and a span of 183 cm (6 ft) was used. This large chord was deliberately selected to obtain a relatively thick boundary layer and to increase the mean velocity deceleration range at the Reynolds numbers of interest. Both of these aspects are of prime concern in this investigation. The airfoil was constructed of a steel skin of 0.5 mm (0.02 in.) thick stretched over a solidified styrofoam core. Its surface was polished, painted with dead-black lacquer and buffed to ensure an extremely smooth surface and to facilitate flow visualization. A final surface relative roughness of about $3x10^{-5}$ was obtained. The solid blockage factor, that was estimated according to the method outlined in References 16 and 17, amounted to 0.0164. In other words, the increase in the freestream velocity due to the solid blocking was 1.64% and, hence, it was neglected. Adjustment of the angle of attack with a resolution of about 0.5° was accomplished by means of a manually operated mechanism. The airfoil was mounted across the wind-tunnel width 23 m (75 ft) downstream of the test-section entrance with its chord at zero angle of attack 61 cm (2 ft) above the floor.

Freestream turbulence was produced in a controlled fashion by means of a particular turbulence-generating grid consisting of 24 vertical cylindrical bars which spanned the entire height of the wind-tunnel. The aluminum rods composing the grid were 1.27 cm (½ in.) in diameter d and were spaced at a center-to-center interval (or mesh length M) of 6.35 cm (2½ in.). Thus, the grid mesh-length to rod-diameter ratio M/d = 5 (or its geometric solidity d/M = 0.20). The vertical orientation of the rods was specifically chosen to produce vorticity (or turbulence) mainly in the x_1-direction as depicted in Fig. 1. This is that particular component of a general three-dimensional vorticity susceptible to undergoing amplification by stretching in the flow situation considered. The turbulence-generating grid was installed 61 cm (24 in. or half chord c/2) upwind of the airfoil. This positioning prevented the total dissipation of turbulence before reaching the airfoil stagnation zone considering its relatively rapid decay downstream of a grid [18].

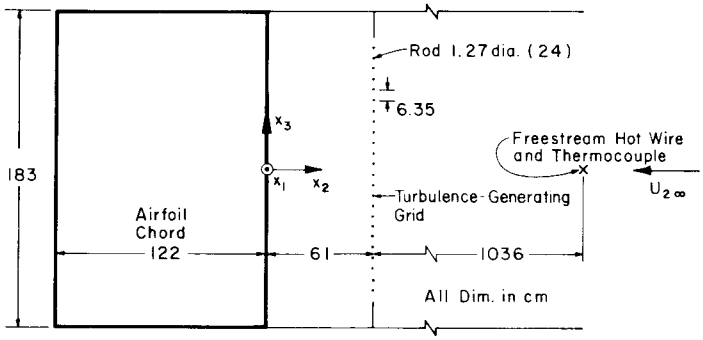

Fig. 2 Sketch of experimental setup.

A computer operated triaxial motorized traversing mechanism was utilized to position any measuring probe with a resolution better than 0.01 mm (0.0004 in.). A schematic diagram of the experimental setup including all important dimensions and the Cartesian system of coordinates used in this experiment are displayed in Fig. 2.

The origin of the system of coordinates is at the airfoil leading edge midspan on the wind-tunnel centerline.

4. EXPERIMENTAL PROCEDURE

This experimental investigation was conducted at subcritical profile-chord Reynolds numbers ranging from 5×10^4 to 2×10^5. The profile-chord Reynolds number Re_c was based on the freestream velocity $U_{2\infty}$ and the airfoil chord (c = 122 cm) in air at 20°C (68°F) (kinematic viscosity $\nu = 1.5\times10^{-5}$ m^2/s (1.6×10^{-4} ft^2/s)). Hence, the corresponding freestream velocity varied from 0.61 to 2.44 m/s (2 to 8 ft/s). In light of the relatively low freestream velocities of interest and in order to simultaneously measure the accompanying turbulence, the freestream conditions upstream of the turbulence-generating grid were continuously monitored by means of a hot-wire anemometer. This freestream hot-wire probe was positioned 61 cm (2 ft) above the wind-tunnel floor at a distance of 10.36 m (34 ft) upwind of the turbulence-generating grid on the wind-tunnel centerline as shown in Fig. 2.

Both the mean velocity $\bar{U}_2$ (the overbar denotes time-averaged value) and the streamwise turbulent velocity u_2 between the turbulence-generating grid and the airfoil leading edge were measured by another single hot-wire anemometer attached to the traversing mechanism. These measurements were performed at 14 stations over a distance of 61 cm (2 ft) along the airfoil stagnation streamline, i.e., along the x_2-axis in the midplane $x_3 = 0$ of the test section. Single copper plated tungsten wires 8.90 μm (0.35 mils) in diameter and about 1000 μm (40 mils) long-i.e., aspect ratio (length-to-diameter ratio) of 114-were employed.

A dual-amplifier constant-temperature hot-wire anemometer unit conceived, designed and built at Colorado State University was utilized [19]. Unique features of this hot-wire anemometer unit permits one to measure turbulence intensity at low velocity with a resolution of about 0.1%. The rms noise level of this hot-wire anemometer unit over its entire frequency bandwidth response, that is 200 kHz, is constant and smaller than about 200 μV. All the details of this hot-wire anemometer unit can be found in Ref. 19. Two identical units, one for the freestream conditions and a second for the measurements between the grid and the airfoil, were used.

Accurate calibration of each hot-wire probe was of prime importance at the low velocities encountered in this experiment. Each calibration was performed at the same temperature as during the test run by means of a standard calibrator (Thermo-Systems Inc., Calibrator, Model 1125). Furthermore, calibration was carried out before each test run and checked afterward. It was reproducible within 1 to 3%. During the calibration the wire was exactly oriented as it would be in the test run to account for free-convection effects. All the measurements were conducted with the hot wire aligned normal to the axial velocity U_2 for maximum output voltage considering its directional sensitivity according to the cosine law [20]. The calibration revealed that the ½-power law-i.e., $\bar{E}^2 \sim \bar{U}^{\frac{1}{2}}$, where the DC output voltage of the unit and the mean velocity (time-averaged velocity) are designated by $\bar{E}$ and $\bar{U}$, respectively-was reasonably satisfied within 2% at all the mean velocities of interest. Then the turbulence intensity Tu, that was computed according to the method outlined in Ref. 21, is given by

$$\frac{u_{rms}}{\bar{U}} = 4B\frac{e_{rms}}{\bar{E}}, \qquad (1)$$

where u_{rms} and e_{rms} are the root-mean-square values of the turbulent velocity u and the fluctuating output voltage e (AC output voltage) of the hot-wire anemometer unit, respectively. In the foregoing equation the hot-wire parameter

$$B = 1/[1-1/(1+m)^2], \qquad (2)$$

and the flow factor

$$m = \Delta\bar{E}/E_o, \qquad (3)$$

in which the velocity induced DC voltage drop $\Delta\bar{E} = \bar{E} - E_o$, and where E_o stands for the DC output voltage in still air (no flow or probe shielded). It is important to point out that Eq. (1) is obtained under the assumption of small fluctuations and it applies when the flow factor $m \geq 0.2$ [21]. The output signal of the hot-wire anemometer unit was continuously recorded on an FM magnetic tape recorder (Ampex Corp., Portable Instrumentation Magnetic Tape Recorder/Reproducer, Model FR 1300) for subsequent reduction and analysis. An efficient method for performing the spectral analysis of the turbulent data using a minicomputer was further advanced [22].

The reliability of a hot-wire measurement is contingent upon the control of the flow temperature. It was maintained constant during the test run over a period of several hours to within 1 to 2°C (1.8 to 3.6°F). The flow temperature was continuously surveyed by means of a thermocouple installed at the same station as the freestream hot-wire probe as shown in Fig. 2. A digital temperature indicator (Doric Scientific Div., Trendicator, Model 400A), whose resolution is 0.1°C (0.18°F), was employed in conjunction with the thermocouple.

5. FLOW VISUALIZATION

A preliminary flow visualization of the turbulent flow patterns near the stagnation zone of the airfoil was undertaken. This preliminary visualization had a twofold goal. To start with, it was conducted in order to develop an expedient visualization technique considering the inherent difficulties associated with flow visualization in a region of relatively high turbulence. With the completion of the method development, the purpose of the visualization was to gain a first physical insight into the stretching of cross-vortex tubes and the existence of a coherent substructure near

the airfoil nose.

This preliminary visualization effort was carried out in a special visualization lowspeed open-circuit wind-tunnel whose dimensions are 61x61x183 cm (2x2x6 ft). A two-dimensional symmetric NACA 65-010 airfoil of both chord and span of 61 cm (2 ft) was used. The visualization was performed at a profile-chord Reynolds number of 2.5×10^4-i.e., at a freestream velocity of 0.61 m/s (2 ft/s)-and at zero angle of attack. Freestream turbulence was produced by means of a grid similar to that described in Sect. 3 which was installed a half chord upwind of the airfoil. After numerous trials, it was concluded that the best visualization is achieved using titanium dioxide white smoke as the tracing agent. An efficient technique along with an adequate apparatus was devised [23]. At the present time, an extensive visualization utilizing the large chord airfoil (see Sect. 3) is being carried out.

Remarkable evidence concerning both the stretching of a cross-vortex tube and the subsistence of a coherent substructure was supplied by the preliminary visualization. Two representative still photographs showing the side and top views of a stretched cross-vortex tube near the airfoil leading edge are given in Figs. 3(a) and 3(b), respectively. The outline of the profile is traced in Fig. 3(a)

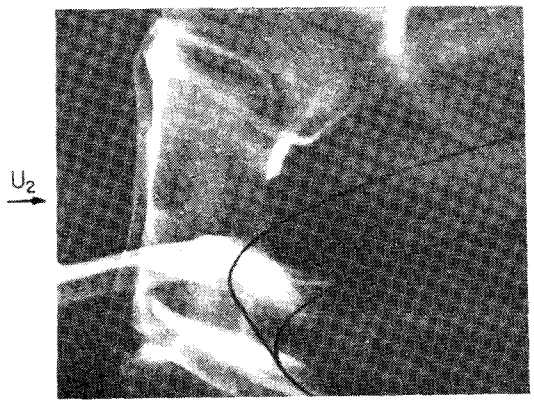

(a) Side view

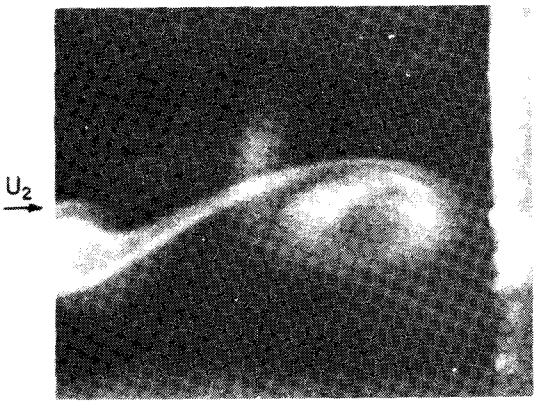

(b) Top view

Fig. 3 Side and top views of the vortex flow pattern near the leading edge of a symmetric NACA 65-010 profile at zero angle of attack at a Reynolds number of 25,000; f/5.6, 1/30 s.

for convenience. Entrainment of the smoke filaments by a standing cross-vortex tube, whose axis is normal to the incident flow (i.e., in the x_3-direction, see Fig. 1), is discernibly noticed in these two stills. Realization of stretching is inferable from the distinctly spiral shape of the cross-vortex tube. The existence of a coherent substructure near the airfoil nose is further indicated by the prominent tubular pattern of the stretched cross--vortex tube. In fact, this tube delineates a cell within the coherent substructure. Digitization of the flow images is currently being conducted using the technique outlined in Ref. 11. Preliminary findings revealed that the length and time scales associated with the stretched cross-vortex tube are, by and large, smaller than their counterparts identified in flow around a circular cylinder [11]. Thus, the preliminary visualization clearly demonstrated that the flow situation was adequate for conducting the investigation of amplification of freestream turbulence.

6. RESULTS

The main objective of this experimental investigation of the evolution of freestream turbulence in flow about a symmetric NACA 65-010 airfoil was to determine its selective amplification induced by the stretching mechanism. This experiment was conducted with the airfoil at zero angle of attack in order to identify the realization of turbulence amplification in the most limiting flow situation. The flow divergence around the airfoil, which controls the stretching of cross-vortex tubes, is the smallest at this angle of attack. Consequently, the stretching is the least and the turbulence amplification is the lowest.

Measurement of the axial (or normal) mean velocity U_2 and, particularly, of the evolution of the axial turbulent velocity u_2 was carried out along the x_2-axis (for the stagnation streamline) at six subcritical profile-chord Reynolds numbers, viz., at $Re_c = 5\times10^3$, 7.5×10^4, 10^5, 1.25×10^5, 1.5×10^5 and 2×10^5. Only a sample of the results at a Reynolds number of 1.5×10^5-viz., at a freestream velocity $U_{2\infty} = 1.83$ m/s (6 ft/s)-are reported herein due to space constraints. Similar results were obtained at the other Reynolds numbers. The system of coordinates used in the presentation of the findings is portrayed in Fig. 2 as previously mentioned. For generality, the results are presented in a dimensionless form and the dimensionless variables, whenever utilized, are denoted by a tilde. The dimensionless axial coordinate is defined by

$$\tilde{x}_2 = x_2/c, \tag{4}$$

where $c = 122$ cm is the airfoil chord. In presenting the results pertinent discussions are interspersed wherever they are deemed helpful for their proper interpretation.

6.1 Mean Velocity Survey

The measured axial mean velocity distribution along the stagnation streamline is displayed in Fig. 4. In this figure the variation of the dimensionless mean velocity, which is defined by

$$\tilde{U}_2 = U_2/U_{2\infty}, \tag{5}$$

where $U_{2\infty} = 1.83$ m/s, is shown omitting the overbar. A gradual decrease followed by an extremely sharp deceleration over a range of 0.02c (2.44 cm (0.96 in.)) upwind of the airfoil stagnation point is discerned. The measurements in the immediate vicinity of the stagnation point within a distance of 0.005c (0.61 cm (0.24 in.)) are accurate to within ± 10%. This is due, in all likelihood, to a slight shift in the position of the stagnation point because of the very presence of the wire. A similar effect is, for instance, reported in Ref. 8. It was further interesting to compare, to a first approximation, the measured mean velocity with that in unbounded potential flow around a symmetric Joukowsky airfoil with a similarly shaped nose-i.e., same curvature of the leading edge-as the present NACA 65-010 airfoil. This theoretical normal mean velocity is given along the stagnation streamline (i.e., along the $\tilde{x}_2$-axis) by

$$U_2/U_{2\infty} = \left[1 - \left(\frac{1+\varepsilon}{\varepsilon - \eta}\right)^2\right] \Big/ \left[1 - 1/\eta^2\right] \quad , \qquad (6)$$

where ε is a dimensionless constant parameter connected to the thickness ratio of the airfoil and η is a dimensionless variable related to the axial coordinate $\tilde{x}_2$. All the details of this computation, that was conducted by means of an adequate Joukowsky transformation [24], are outlined in Ref. 23. The variation of this theoretical normal velocity is also shown in Fig. 4. A reasonable agreement in the variations of both theoretical and measured velocities

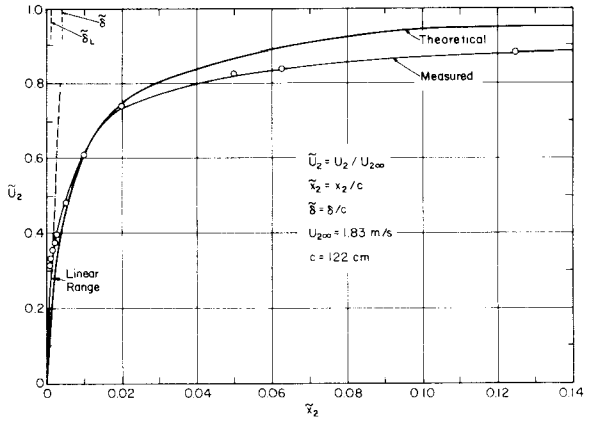

Fig. 4 Measured and theoretical axial mean velocity distribution along the stagnation streamline.

within a difference of 8%, at most, is observed. Particularly revealing is the similarly steep deceleration of both velocities close to the airfoil stagnation point, i.e., within a distance of 0.02c from the airfoil leading edge.

The normal velocity decelerates linearly in the vicinity of the stagnation point of a plane flat plate in crossflow according to the relationship $U_2 = -ax_2$ based on potential flow theory [25]. A similar velocity deceleration is considered in this flow around an airfoil. Then the constant rate of deceleration a is simply given by the slope of the normal velocity within its linear deceleration range, i.e., $a = dU_2/dx_2$, omitting the negative sign for convenience. Based on the measured sharp decrease in the mean velocity, it was estimated that its linear deceleration range extends over a distance of about 0.005c from the stagnation point. Most of the stretching action is supposedly confined within this linear range [5]. The value of the stagnation-flow constant a computed from the average slope of the linear normal velocity that is indicated by a dash-dot line in Fig. 4, was 300 s^{-1}. Its value is about 20 to 30 times larger than in flow about a flat plate at the same Reynolds number [6]. Both the relatively short extent of the linear range and the corresponding large value of the stagnation-flow constant reflect the fast flow divergence about the airfoil.

The theoretical thickness of the laminar boundary layer at the stagnation point was computed using the Hiemenz flow relation $\delta_L = 2.4(\nu/a)^{1/2}$ [6,25] and the measured value of the constant a. It was about 0.53 mm (0.021 in.) or in terms of the airfoil chord 0.0004c. Preliminary survey of the actual turbulent boundary layer indicated that its thickness δ was roughly 4 to 5 times greater than that of the theoretical laminar one, i.e., 2.12 to 2.65 mm (0.083 to 0.104 in.) or referred to the airfoil chord 0.0017 to 0.0022c thick. A similar result was found in flow normal to a flat plate where the thickness of the turbulent boundary layer was about twice that of the theoretical laminar one [6]. Both the theoretical laminar and actual turbulent boundary-layer thicknesses made dimensionless by the airfoil chord c-i.e., $\tilde{\delta}_L = \delta_L/c$ and $\tilde{\delta} = \delta/c$ -are marked off by dashed lines in Fig. 4. The neutral wavelength (or scale) of this flow was further evaluated using the actual value of the stagnation-flow constant a by means of the relationship $\lambda_o = 2\pi(\nu/a)^{1/2}$ [5]. A value of 1.40 mm (0.055 in.) or 0.00115 of the airfoil chord was obtained. It is interesting to point out that this neutral scale is about 5 times smaller than its counterpart in the case of a flat plate in crossflow [6].

6.2 Turbulence Amplification

Turbulence approaching a body experiences amplification due to the stretching of oncoming cross-vortex tubes as illustrated in Fig. 1. The stretching is triggered and governed by the flow divergence around the body and, hence, the amplification of turbulence depends upon how the body excites this mechanism. It was, consequently, imperative to learn the evolution of the grid-produced turbulence in the absence of the airfoil for ascertaining the amplification induced by the latter. Particularly important was to find out the level of turbulence close to where the airfoil was supposed to be located downstream of the grid since most of the stretching transpires within this region.

Background Turbulence

The intensity of the grid-produced axial turbulent velocity u_{2b} was monitored over a distance greater than 25 mesh lengths (158.75 cm (62.50 in.); mesh length M = 6.35 cm, see Sect. 3) downstream of the grid in the absence of the airfoil at freestream velocities corresponding to all the profile-chord Reynolds numbers of interest. This background axial turbulence intensity, based on the freestream velocity $U_{2\infty}$, is expressed by

$$Tu_b = (\overline{u_{2b}^2})^{1/2}/U_{2\infty} \quad , \qquad (7)$$

in which u_{2b}^2 is the mean-square value of the axial turbulent velocity. These measurements were performed at midmesh-i.e., at a distance of 3.175 cm (1¼ in.) from the center of either rod-along the wind-tunnel centerline (along the x_2-axis). The variation of the background axial turbulence intensity with increasing distance downstream of the turbulence-generating grid monitored at a constant freestream velocity $U_{2\infty} = 1.83$ m/s is depicted in Fig. 5. This freestream velocity corresponds to a profile-chord Reynolds number of 1.5×10^5. The grid Reynolds numbers based on either its mesh length M or the rod diameter d, i.e., Re_M or Re_d, were 7,700 and 1,500, respectively, at this particular freestream velocity. In addition to the distance in terms of the airfoil axial coordinate $\tilde{x}_2$, the dimensionless longitudinal distance $\tilde{x}_2'$ measured from the grid in terms of the mesh length M-i.e., $\tilde{x}_2' = (x_{2g} - x_2)/M$, where x_{2g} (0.5c) defines the upwind grid position with respect to the airfoil-is shown in Fig. 5. Furthermore, the airfoil is also portrayed in this figure for convenience.

The background axial turbulence intensity exhibited with increasing downstream distance from the grid a strikingly similar variation to that obtained for an ordinary square-mesh grid at a comparable grid-mesh Reynolds number Re_M [18]. Close to the grid, the turbulence intensity increased initially to a level of about 5.4% over an interval of 5 mesh lengths (31.75 cm (12.50 in.)). With further increase in the axial distance, the turbulence intensity decayed smoothly to a level lower than 2%

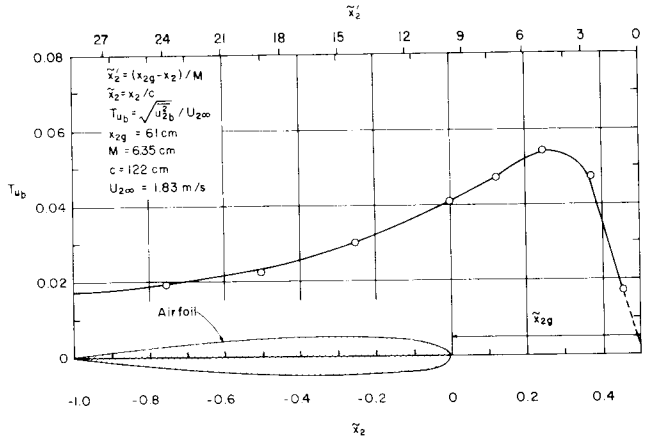

Fig. 5 Background turbulence intensity variation with increasing axial distance from the turbulence-generating grid.

at 27 mesh lengths from the grid (171.45 cm (67.50 in.)). Insofar as the stretching action is concerned, an axial extent upwind of the airfoil position extending over a span of at least 10 times the linear velocity deceleration range-i.e., $\tilde{x}_2 = 0$ to 0.05 (0 to 6.10 cm (0 to 2.40 in.))-is of main interest. The background turbulence intensity changed within this domain from 4.3 to 4% for $\tilde{x}_2$ decreasing from 0.05 to 0 as observed in Fig. 5. It is interesting to point out that an equivalent level of turbulence underwent significant amplification in the case of a flat plate in crossflow [6]. The important aspect of the turbulence produced by the particular grid used is its generally analogue evolution to that generated by a common square-mesh grid. Thus, this background turbulence can serve as an adequate reference for assessing the stretching and, in particular, the turbulence amplification.

Turbulence in Flow About the Airfoil

A detailed survey of the turbulent energy of the axial fluctuating velocity u_2 along the stagnation streamline with the airfoil present was conducted simultaneously with the measurement of the axial mean velocity. It is important to note that the sole nonvanishing turbulent velocity component along the stagnation streamline is the axial (or normal) due to symmetry considerations [6]. The axial (or streamwise) turbulent energy-i.e., the mean-square value $\overline{u_2^2}$ of the axial turbulent velocity-was computed from the turbulence intensity and axial mean velocity data. To start with, the streamwise turbulent energy decayed in a usual manner to a minimum level with increasing distance from the grid. As the airfoil is neared and the flow divergence starts off, the turbulent energy underwent gradual amplification owing to the action of the stretching. It is consequently sensible to refer the streamwise turbulent energy to its minimum value upwind of the airfoil in order to readily assess the level of amplification as the airfoil leading edge is approached. Then the dimensionless streamwise turbulent energy is defined by

$$\tilde{\overline{u_2^2}} = \overline{u_2^2}/\overline{u_{2min}^2} , \qquad (8)$$

where $\overline{u_{2min}^2}$ is the minimum turbulent energy upwind of the airfoil.

A typical distribution of the dimensionless streamwise turbulent energy measured along the stagnation streamline at a Reynolds number of 1.5×10^5 is displayed in Fig. 6. The minimum turbulent energy $\overline{u_{2min}^2}$, that was about 100 cm^2/s^2 (0.108 ft^2/s^2), was monitored at $\tilde{x}_2 = 0.05$ or 8.65 mesh lengths (54.90 cm (21.60 in.)) downstream of the grid. This minimum turbulent energy is viewed as the critical turbulence as regards the amplification. The streamwise turbulent energy gradually

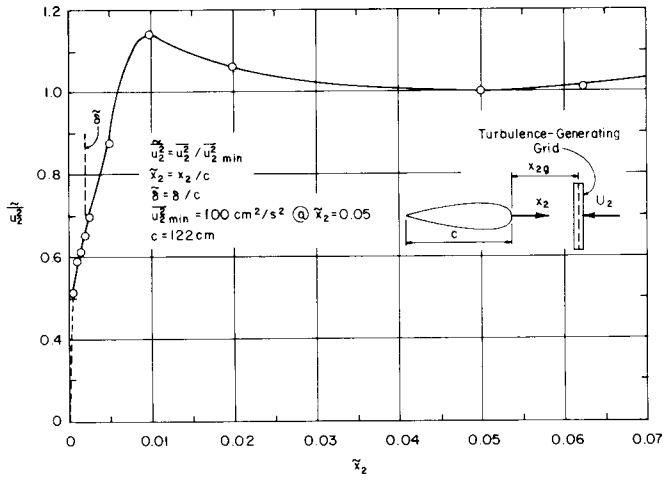

Fig. 6 Streamwise turbulent energy variation along the stagnation streamline.

reached a maximum of about 1.14 over an interval extending from $\tilde{x}_2 = 0.05$ to 0.01 (6.10 to 1.22 cm (2.40 to 0.48 in.)). This maximum amplification of

14% occurred at a distance of 0.01c that is twice the linear range (0.005c) and about five times the boundary-layer thickness (0.002c). The latter is marked off by a dashed line denoted $\tilde{\delta}$ in Fig. 6. Inside the boundary-layer the turbulent energy decreased toward zero at the airfoil stagnation point since there the fluctuating velocity vanishes. The essential features of the turblent energy amplification are its onset at a distance roughly 10 times the linear range and the realization of its peak upwind of both the linear range and the boundary-layer. Thus, the stretching action extends far beyond the linear velocity deceleration domain and, moreover, the turbulence amplification is apparently not associated with any instability within the boundary layer.

The stretching of cross-vortex tubes and the accompanying amplification of turbulence are spurred by the presence of the airfoil. Estimation of the stretching effect is then achieved by comparing the actual streamwise turbulent energy $\overline{u_2^2}$ in the presence of the airfoil to its counterpart when the airfoil is absent. The latter is the background axial turbulent energy $\overline{u_{2b}^2}$ produced by the turbulence-generating grid at exactly the same freestream velocity as that with the airfoil present. To that end, the amplification factor of the streamwise turbulent energy, which is represented by their ratio

$$A_e = \overline{u_2^2}/\overline{u_{2b}^2} \ , \qquad (9)$$

was computed along the stagnation streamline (the x_2-axis). The background turbulent energy was evaluated, in the same manner as the actual one, from the background turbulence intensity and the mean velocity data.

The variation of the streamwise turbulent energy amplification factor along the stagnation streamline at a Reynolds number of 1.5×10^5 is portrayed in Fig. 7. Its corresponding background

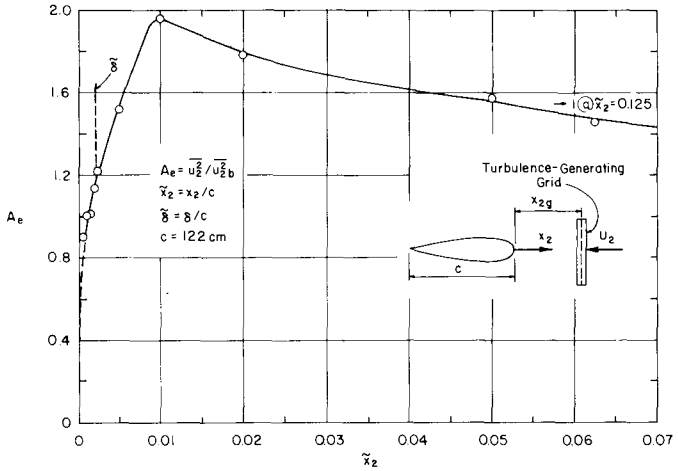

Fig. 7 Variation of amplification factor of streamwise turbulent energy with distance from airfoil leading edge.

axial turbulence intensity is shown in Fig. 5. Significant evidence as regards the amplification of incident turbulence induced by the stretching action is revealed by the variation of the amplification factor. The actual turbulent energy $\overline{u_2^2}$ became greater than the background one starting off from $\tilde{x}_2 = 0.125$ (15.25 cm (6 in.)). This station, where $A_e = 1.0$ and which is not shown in Fig. 7, is thus at a distance of 25 times the linear range from the airfoil. As the airfoil is neared, a continuous augmentation in the amplification factor is distinctly observed. Even the minimum actual turbulent energy, that was recorded at $\tilde{x}_2 = 0.05$ (see Fig. 6), was about 57% higher than the corresponding background turbulent energy. The stretching produces amplification with respect to the background turbulence over an extent considerably larger than the linear range. However, the level of amplification at such a great distance from the body depends upon the balance between the stretching effect and the viscous dissipation. This balance has yet to be explored.

A maximum amplification factor of 1.96 was recorded at the station of greatest actual turbulent energy, i.e., at $\tilde{x}_2 = 0.01$ (see Fig. 6). Thus, the stretching caused by the airfoil led to a maximum amplification of almost 100% with respect to the background level. It is noteworthy to point out that the stretching in this flow situation is mainly a consequence of the streamwise biased tilting of the cross-vortex tubes considering the fast rate of flow divergence around the airfoil. This tilting induced stretching has not yet been adequately investigated.

6.3 Discrete Turbulent Energy

One of the most important features of the stretching mechanisms is the selective amplification of turbulent energy at scales larger than the neutral scale of the stagnation flow [3,5]. At these scales turbulent energy accumulates more rapidly than it dissipates by viscous action. A detailed survey of the turbulent energy spectra of the axial turbulent velocity along the stagnation streamline was therefore carried out for assessing the amplification of turbulent energy at such scales. To start with, the turbulent energy frequency spectra-i.e., $\overline{u_2^2}(n)$, where n is the frequency-were obtained at each station on the stagnation streamline [22]. For each frequency n a corresponding scale λ was introduced, based on the frozen pattern assumption [26], by using the relation

$$\lambda = U_2/n, \qquad (10)$$

where U_2 is the local mean velocity. The total streamwise turbulent energy at a fixed point-i.e., the mean-square value of the fluctuating velocity-is then expressed by

$$\overline{u_2^2} = \sum_{i=1}^{\infty} \overline{u_2^2}(\lambda_i), \qquad (11)$$

in which $\overline{u_2^2}(\lambda_i)$ is that portion of the total turbulent energy concentrated at an eddy of scale λ_i, i.e., the discrete streamwise turbulent energy. In fact, the foregoing equation describes the scale (or eddy) resolution of the turbulent spectrum. This representation permits one to examine the change in turbulent energy at any desired scale as it is conveyed toward the body and, for that matter, the airfoil stagnation point. The discrete turbulent energy at any particular scale is simply derived from the turbulent spectra at a succession

of positions along the stagnation streamline (the x_2-axis).

A sample of the variations along the x_2-axis of the discrete streamwise turbulent energy at three selected scales larger than the neutral one obtained at a Reynolds number of 1.5×10^5 is exhibited in Fig. 8. These three scales are λ = 4, 10 and 40 mm (0.16, 0.39 and 1.57 in.) and, hence, λ/λ_o = 2.86, 7.14 and 28.57 since the neutral wavelength of the vorticity-amplification theory λ_o = 1.40 mm (see Sect. 6.1) at this Reynolds number. In order to readily ascertain the strength of the amplification, the discrete turbulent energy at each scale $\overline{u_2^2}(\lambda)$ is referred to its level $\overline{u_{20}^2}(\lambda)$ at the station of minimum total turbulent energy, i.e., $\overline{u_2^2}(\lambda)$ at $\tilde{x}_2$ = 0.05 (see Sect. 6.2). Then the amplification of discrete turbulent energy at each scale λ is given by

$$\overline{\tilde{u}_2^2}(\lambda) = \overline{u_2^2}(\lambda)/\overline{u_{20}^2}(\lambda) \qquad (12)$$

Realization of noticeable amplification of discrete turbulent energy is clearly discerned at all three selected scales shown in Fig. 8. The amplification transpired starting off from a distance of nearly 0.02c from the airfoil with most of it occurring within a range of 0.01c. Thus, the amplification of discrete turbulent energy extends, as for the total turbulent energy, over an interval much longer than the linear velocity deceleration

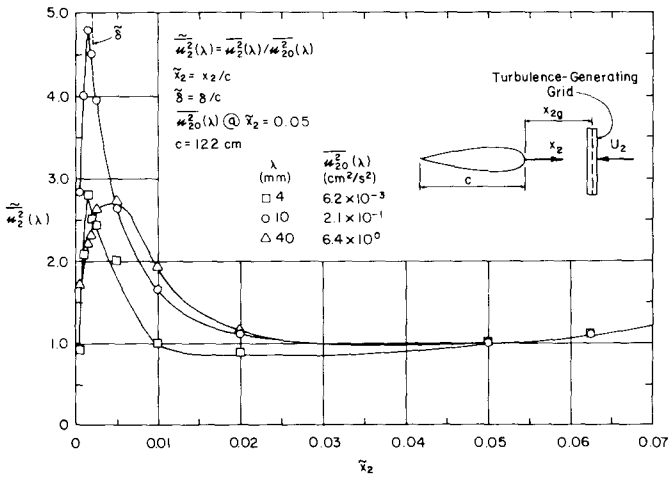

Fig. 8 Change in discrete turbulent energy at three scales with distance from airfoil leading edge.

range. The greatest amplification in the discrete turbulent energy was found at a scale that is neither the largest nor the smallest. At this particular scale of 10 mm, that is 7.14 times the neutral one, an almost fivefold amplification was monitored. At the other two scales, that are about 2.86 and 28.57 times larger than the neutral one, an amplification of only about 2.75 times was, on the other hand, recorded. Essentially, the scale at which the greatest amplification occurred is the most amplified scale λ_m induced by the stretching in this particular stagnation flow. A similar most amplified scale was detected in crossflow about a flat plate [6]. This scale is representative of the energy-containing eddies within the standing coherent substructure near the airfoil stagnation zone.

It is, further, interesting to notice that the discrete turbulent energy reached its maximum amplification at all scales in the vicinity of the outer edge of the actual boundary layer. This is particularly manifested for the most amplified scale λ_m whose peak is almost at the outer edge of the boundary layer. The thickness of the boundary layer (roughly 0.002c) is indicated by a dashed line designated $\tilde{\delta}$ in Fig. 8 for convenience. Inside the boundary layer the discrete turbulent energy gradually decayed to zero at the airfoil stagnation point.

Another germane point is that the most amplified scale was, as a matter of fact, commensurable with the boundary-layer thickness. It was about four times the latter and it averaged roughly 19 times the thickness of the theoretical laminar boundary layer. One thus can conjecture that this amplified turbulence interacts with the boundary layer and affects its characteristics. This interaction is, in all likelihood, responsible for the turbulent nature of the boundary layer at the prevailing subcritical Reynolds number.

7. CONCLUDING REMARKS

The results presented in this work clearly testify to the realization of amplification of freestream turbulence at scales larger than the neutral wavelength in flow about an airfoil. This selective amplification of turbulence is induced by the stretching of oncoming cross-vortex tubes which is, in turn, stimulated by the flow divergence around the airfoil according to the vorticity-amplification theory. Even in the limiting situation of a symmetric airfoil at zero angle of attack in cross-flow reported here, where the stretching is the least since the flow divergence is the smallest, significant amplification transpired.

This investigation was carried out at a subcritical profile-chord Reynolds number of 1.5×10 with freestream turbulence superimposed by means of an adequate turbulence-generating grid. A relatively short linear velocity deceleration range along with a high stagnation flow constant were found. They attest to the rapid rate of flow divergence around the airfoil. Amplification of the total streamwise turbulent energy occurred constantly over an extent much larger than the linear velocity deceleration range. A maximum amplification ratio of the total turbulent energy of 1.14, relative to its minimum level, was monitored outside of both the linear range and the boundary layer. These findings plainly suggest that the turbulence amplification is not affected by any boundary-layer instability. Noteworthy substantiation concerning the stretching effect was furnished by the amplification factor that expresses the ratio of the actual turbulent energy to its background counterpart. The former is the turbulent energy in the presence of the airfoil while the latter was monitored with the airfoil absent. Amplification factors up to almost 100% were obtained notwithstanding that the stretching is the least in this flow situation.

Preferred amplification of turbulence at scales larger than the neutral wavelength, as predicted by the vorticity-amplification theory, was distinctly demonstrated by the variation of the discrete turbulent energy. The latter was deduced from the

turbulent energy spectra at a succession of positions by means of their scale resolution. At all the scales examined substantial amplifications of the discrete turbulent energy were found with the peaks close to the outer edge of the boundary layer. Particularly significant was the detection of a most amplified scale at which a maximum amplification of almost fivefold (500%) in the discrete turbulent energy was recorded. This scale, that is neither the largest nor the smallest, is characteristic of the coherent substructure near the airfoil stagnation zone and, concurrently, commensurate with the boundary-layer thickness. It is conjectured that the penetration of this amplified turbulence into the boundary layer is responsible for fostering its change from laminar to turbulent at the prevailing subcritical Reynolds number.

Acknowledgment. The work reported here is part of a research program on the structure of turbulence and the effect of turbulence upon the separation in flow about aerodynamic surfaces such as airfoils and compressor blading. Sponsoring of this research program by NASA Lewis Research Center is gratefully acknowledged.

REFERENCES

1. Piercy, N. A. and Richardson, E. G., "The variation of velocity amplitude close to the surface of a cylinder moving through a viscous fluid," Phil. Mag., Vol. VI, 1928, pp. 970-977.

2. Kestin, J. and Maeder, P. F., "Influence of turbulence on the transfer of heat from cylinders," NACA TN 4018, 1957.

3. Sutera, S. P., Maeder, P. F. and Kestin, J., "On the sensitivity of heat transfer in the stagnation-point boundary layer to freestream vorticity," J. Fluid Mech., Vol. 16, Part 4, 1963, pp. 497-520.

4. Sutera, S. P., "Vorticity amplification in stagnation-point flow and its effects on heat transfer," J. Fluid Mech., Vol. 21, Part 3, 1965, pp. 513-534.

5. Sadeh, W. Z., Sutera, S. P. and Maeder, P. F., "Analysis of vorticity amplification in the flow approaching a two-dimensional stagnation point," Z. angew. Math. Phys. (ZAMP), Vol. 21, Fasc. 5, 1970, pp. 699-716.

6. Sadeh, W. Z., Sutera, S. P. and Maeder, P. F., "An investigation of vorticity amplification in stagnation flow," Z. angew. Math. Phys. (ZAMP), Vol. 21, Fasc. 5, 1970, pp. 717-742.

7. Kestin, J. and Wood, R. T., "On the stability of two-dimensional stagnation flow," J. Fluid Mech., Vol. 44, Part 3, 1970, pp. 461-479.

8. Bearman, P. W., "Some measurements of the distortion of turbulence approaching a two-dimensional bluff body," J. Fluid Mech., Vol. 53, Part 3, 1972, pp. 451-467.

9. Hunt, J. C. R., "A theory of turbulent flow round two-dimensional bluff bodies," J. Fluid Mech., Vol. 61, Part 4, 1973, pp. 625-706.

10. Traci, R. M. and Wilcox, D. C., "Freestream turbulence effects on stagnation point heat transfer," AIAA Journal, Vol. 13, No. 7, 1975, pp. 890-896.

11. Sadeh, W. Z. and Brauer, H. J., "A visual investigation of turbulence in stagnation flow about a circular cylinder," to be published in the Journal of Fluid Mechanics.

12. Sadeh, W. Z., Brauer, H. J. and Sullivan, P. P., "Freestream turbulence effect on laminar separation on a circular cylinder," to be published.

13. Piercy, N. A. and Richardson, E. G., "The turbulence in front of a body moving through a viscous fluid," Phil. Mag., Vol. IX, 1930, pp. 1038-1040.

14. Schlichting, H. and Das, A., "On the influence of turbulence level on the aerodynamic losses of axial turbomachines," Flow Research on Blading, ed. Dzung, L. S., Elsevier Publishing Co., Amsterdam, The Netherlands, 1970, pp. 322-371.

15. Kiock, R., "Einfluss des turbulenzgrads auf die aerodynamischen eigenschaften von ebenen verzögerungsgittern," Forschung im Ingenieurwesen, Vol. 39, No. 1, 1973, pp. 17-28.

16. Allen, H. J. and Vincenti, W. G., "Wall interference in a two-dimensional flow wind tunnel, with consideration of the effect of compressibility," NACA TR 782, 1944.

17. Pope, A. and Harper, J. J., Low-Speed Wind Tunnel Testing, John Wiley & Sons, Inc., New York, New York, 1966, pp. 305-311.

18. Hinze, J. O., Turbulence, 2nd ed., McGraw-Hill Book Co., New York, New York, 1975, pp. 269-271.

19. Sadeh, W. Z. and Finn, C. L., "A dual-amplifier hot-wire anemometer," Proceedings, Fifth Biennial Symposium on Turbulence, University of Missouri-Rolla, Rolla, Missouri, 1977, eds. Patterson, G. K. and Zakin, J. L., Science Press, Princeton, New Jersey, 1979, pp. 259-263.

20. Kovasznay, L. S. G., "Hot-wire method," Physical Measurement in Gas Dynamics and Combustion, ed. Landenburg, R. W. et al., University Press, Princeton, New Jersey, 1954, Part 2, Art. F, pp. 219-285.

21. Sadeh, W. Z., Maeder, P. F. and Sutera, S. P., "A hot-wire method for low velocity with large fluctuations," Review of Scientific Instruments, Vol. 41, No. 9, 1970, pp. 1295-1298.

22. Sadeh, W. Z. and Sullivan, P. P., "A method for on-line spectral analysis of turbulent flow data," to be published.

23. Sadeh, W. Z. and Sullivan, P. P., "Turbulence in flow about a symmetric airfoil," NASA CR, to be published.

24. Kármán, Th. von and Burgers, J. M., "General aerodynamic theory-perfect fluids," Aerodynamic Theory, ed. Durand, W. F., Vol. II, Div. E.,

Dover Publications, Inc., New York, New York, 1963, pp. 58-74.

25. Schlichting, H., Boundary-Layer Theory, 7th ed., McGraw-Hill Book Co., New York, New York, 1979, pp. 95-99.

26. Taylor, G. I., "The spectrum of turbulence," Proc. Roy. Soc. A, Vol. CLXIV, 1938, pp. 476-490.